Nat. Hazards Earth Syst. Sci. Discuss., doi:10.5194/nhess-2017-41, 2017
Manuscript under review for journal Nat. Hazards Earth Syst. Sci.
Published: 6 February 2017

Natural Hazards and Earth System Sciences
Open Access
Discussions

Integrating faults and past earthquakes into a probabilistic seismic hazard model for peninsular Italy

Alessandro Valentini[1], Francesco Visini[2] and Bruno Pace[1]

[1] DiSPUTer, Università degli Studi "Gabriele d'Annunzio", Chieti, Italy

[2] Istituto Nazionale di Geofisica e Vulcanologia, L'Aquila, Italy

Abstract

Italy is one of the most seismically active countries in Europe. Moderate to strong earthquakes, with magnitudes of up to ~7, have been recorded on many of active faults in historical times. Currently, probabilistic seismic hazard assessments in Italy are mainly based on area source models, in which the seismicity is modelled on a number of seismotectonic zones and the occurrence of earthquakes is assumed to be uniform. However, in the last decade, efforts have increasingly been directed towards using fault sources in seismic hazard models to obtain more detailed and possibly more realistic patterns of ground motion. In our model, we used two categories of earthquake sources. The first involves active faults, and fault slip rates were used to quantify the seismic activity rate. We produced an inventory of all fault sources, with details on their geometric, kinematic and energetic properties. The parameters are used to compute the total seismic moment rate for each fault. We evaluated the magnitude-frequency distributions of each fault source using two models, a characteristic Gaussian model centred on the maximum magnitude and a Truncated Gutenberg-Richter model. The second earthquake source category involves distributed seismicity, and a fixed-radius smoothed approach and a historical catalogue were used to evaluate seismic activity. Under the assumption that deformation is concentrated along faults, we combined the earthquakes derived from the geometry and slip rates of active faults with the earthquakes from the spatially smoothed earthquake sources and assumed that the smoothed seismic activity in the vicinity of an active fault gradually decreases by a fault-size driven factor. We computed horizontal peak ground acceleration maps for return periods of 475 and 2,475 yr. Although the range and gross spatial distribution of the expected accelerations obtained here are comparable to those obtained through methods involving seismic catalogues and classical zonation models, the spatial pattern of our model is far more detailed. Our model is characterized by areas that are more hazardous and that correspond to mapped active faults, while the previous models yield expected accelerations that are almost uniformly distributed across large regions. In addition, we conducted sensitivity tests to determine the impact on the hazard *results of the earthquake rates derived from two magnitude-frequency distribution models for faults and to determine the relative contributions of faults versus distributed seismic activity. We think our model represents an advance for Italy in terms of input data (quantity and quality) and methodology in the field of the fault-based regional seismic hazard modelling.*

1. Introduction

In this paper, we present the results of a new probabilistic seismic hazard (PSH) model for Italy that includes significant advances in the use of integrated active fault and seismological data in seismic hazard estimations. The use of active faults as an input for PSH analysis is a consolidated approach in many countries characterized by high strain rates and seismic releases, as shown by, for example, Field et al. (2015) in California and Stirling et al. (2012) in New Zealand. However, in recent years, active fault data have also been successfully integrated into PSH assessments in regions with moderate-to-low strain rates, such as SE Spain (e.g., Garcia-Mayordomo et al., 2007), France (e.g., Scotti et al., 2014), and central Italy (e.g., Peruzza et al., 2011). In Europe, a working group of the European Seismological Commission, named *Fault2SHA*, has recently discussed fault-based seismic hazard modelling (https://sites.google.com/site/linkingfaultpsha/home).

Combining seismic hazards from active faults with background sources is also one of the main issues in this type of approach. Although the methodology remains far from identifying a standard procedure, common approaches combine active faults and background sources by applying a threshold magnitude, generally between 5.5 and 7, above which seismicity is modelled as occurring on faults and below which seismicity is modelled via a smoothed approach (e.g., Akinci et al., 2009), area sources (e.g. the so-called FSBG model in SHARE) or a combination of the two (Field et al., 2015; Pace et al., 2006).

Currently in Italy the national probabilistic seismic hazard model for building code (Stucchi et al., 2011) is based on area sources and classical Cornell approach (Cornell, 1968), in which the occurrence of earthquakes is assumed to be uniform on the defined seismotectonic zones. However, we think that more efforts have to be directed towards using geological data (e.g. fault sources and paleoseismological information) in PSH models, obtaining more detailed and possibly more realistic patterns of ground motion, in order to improve the reliability of seismic hazard

Nat. Hazards Earth Syst. Sci. Discuss., doi:10.5194/nhess-2017-41, 2017
Manuscript under review for journal Nat. Hazards Earth Syst. Sci.
Published: 6 February 2017

Natural Hazards and Earth System Sciences Discussions

assessments. In fact, as highlighted by the 2016-2017 seismic sequences in central Italy, a zone-based PSH is not able to model locally spatial variation of ground motion (Meletti et al., 2016), whereas a fault-based model can also be give insights to perform aftershock time-dependent PSH analysis (Peruzza et al, 2016).

2. Source Models

Two earthquake-source models are considered in this work. The first one is a fault source model that is based on active faults and uses the geometries and slip rates of the known active faults to compute activity rates over a certain range of magnitude. The second one is a classical smoothed approach that can take into account rates of expected earthquakes from a minimum moment magnitude (Mw) of 4.5 but excludes earthquakes associated with known faults based on a modified earthquake catalogue. In the following subsections, we describe the two source models and how they are combined into the PSH model.

2.1 Fault Source Model

Fault source models are useful for seismic hazard studies, and we define one for Italy via compilation and synthesis of neotectonic and seismotectonic data from approximately 90 published studies on 110 faults across Italy. The resulting database of normal and strike-slip active and seismogenic faults in Italy (Fig. 1, Table 1 and 2; see supplement files) includes all the available geometric, kinematic, slip rate and earthquake source-related information derived from a synthesis of published works over the last twenty years (see supplements for complete references). In the case of missing data for the geometric parameters, as dip or rake, we assumed typical dip and rake values of 60° and -90, respectively, for normal faults and 90° and 0 or 180, respectively, for strike-slip faults. In this paper, only normal and strike-slip faults are used in the fault source model; thrust faults could be considered in a future study. The upper and lower boundaries of the seismogenic thickness are mainly derived from the analysis of Stucchi et al. (2011) for the Italian national seismic hazard model and locally refined by more detailed studies (Boncio et al., 2011; Peruzza et al., 2011; Ferranti et al., 2014).

Nat. Hazards Earth Syst. Sci. Discuss., doi:10.5194/nhess-2017-41, 2017
Manuscript under review for journal Nat. Hazards Earth Syst. Sci.
Published: 6 February 2017

Natural Hazards and Earth System Sciences
Open Access
Discussions

Based on the compiled database, we explored in detail three main issues associated with defining a fault source model: the slip rate evaluation, the segmentation model and the expected seismicity rate calculation.

2.1.1 Slip rates

Slip rates control fault-based seismic hazards (Main, 1996, Roberts et al., 2004; Bull et al., 2006; Visini and Pace, 2014) and provide a time scale with which to assess the mechanisms operating during continental deformation (e.g., Cowie et al., 2005). Moreover, long-term observation of faults in various tectonic contexts has shown that slip rates vary in space and time (e.g. Bull et al., 2006; Nicol et al., 2006, 2010, McClymont et al., 2009; Gunderson et al., 2013; Benedetti et al., 2013), and numerical simulations (e.g. Robinson et al., 2009; Cowie et al., 2012; Visini and Pace, 2014) suggest that variability mainly occurs in response to interactions between adjacent faults. Therefore, understanding the temporal variability in fault slip rates is a key point to understanding the earthquake recurrence rates and their variability.

In this work, minimum and maximum slip rate values are derived based on approximately 65 available neotectonics, palaeoseismology and seismotectonics papers (see supplement files). To evaluate the long-term slip rate, which is representative of the average slip behaviour, and its variability through time, we use slip rates determined for different time scales for the same fault (e.g., at the decadal scale based on geodetic data or at longer scales based on the displacement of Holocene or Plio-Pleistocene horizons). Because a direct comparison of slip rates over different time intervals obtained by different methods may be misleading (Nicol et al., 2009), we cannot exclude the possibility that epistemic uncertainties could affect the original data in some cases. The discussion of these possible biases and their evaluation via statistically derived approaches (e.g. Gardner et al., 1987; Finnegan et al., 2014; Gallen et al., 2015) is beyond the scope of this paper and will be explored in future work.

Because 28 faults had no measured slip (or throw) rate (Fig. 1a), we propose a statistically derived approach to assign a slip rate to these faults. On the basis of the slip rate spatial distribution shown in Figure 1b, we subdivided the fault database into three large regions – Northern Apennines, Central-Southern Apennines and Calabria-Sicilian coast – and analysed the slip rate distribution in these three areas. In Figure 1b, the slip rates tend to increase from north to south. The fault slip rates in the Northern Apennines range from 0.3 to 0.8 mm/yr, with the most common being approximately 0.5-0.6 mm/yr; the slip rates in the Central-Southern Apennines range from 0.3 to 1.0, with the most common being approximately 0.3 mm/yr; and the slip rates in the southern area (Calabria and Sicily) range from 0.9 to 1.8, with the most common being approximately 0.9 mm/yr.

The first step in assigning an average slip rate and a range of variability to the faults with unknown values is to identify the most representative distribution among known probability density functions using the slip rate data from each of the three areas. We test five well-known probability density functions (*Weibull*, *Normal*, *Exponential*, *Inverse Gaussian* and *Gamma*) against mean slip rate observations. The resulting function with the lowest log-likelihood is the Normal function for all three areas. The mean value of the *Normal* distribution is assigned to the faults with unknown values. We assign a value of 0.58 mm/yr to faults in the Northern area, 0.64 mm/yr to faults in the Central-Southern area, and 1.10 mm/yr to faults in the Calabria-Sicilian area. To assign a range of slip rate variability to each of the three areas, we test the same probability density functions against slip rate variability observations. Similar to the mean slip rate, the probability density function with the lowest log-likelihood is the *Normal* function for all the three areas. We assign a value of 0.25 mm/yr to the faults in the Northern area, 0.29 mm/yr to the faults in the Central-Southern area, and 0.35 mm/yr to the faults in the Calabria-Sicilian area.

2.1.2 Segmentation rules

An important issue in the definition of a fault source model is the formulation of segmentation rules. In fact, the question of whether structural segment boundaries along multi-segment active faults act as persistent barriers to a single rupture is critical to defining the maximum seismogenic potential of fault sources. In our case, the rationale behind the definition of a fault source is based on the assumption that the geometric and kinematic features of a fault source are the expression of its seismogenic potential and that its dimensions are compatible to host major (Mw ≥

5.5) earthquakes. Therefore, a fault source is a fault or an ensemble of faults that slip together during an individual major earthquake. A fault source is defined by a *seismogenic master fault* and its surface projection (Fig. 2a). *Seismogenic master faults* are separated from each other by first-order structural or geometrical complexities. Following the suggestions by Boncio et al. (2004) and Field et al. (2015), we imposed the following segmentation rules on our case study: (i) 4-km fault gaps among aligned structures; (ii) sharp bends or intersections with cross structures (often transfer faults) extending 4 km along strike and oriented at nearly right angles to the intersecting faults; (iii) overlapping or underlapping en echelon arrangements with separations between faults of 4 km; (iv) bending ≥ 60° for more than 4 km; (v) average slip rate variability along strike greater than or equal to 50%; and (vi) seismogenic thickness greater than 5 km among aligned structures. Example applications of the above rules are illustrated in Figure 2a.

By applying the above rules to our fault database, the 110 faults yielded 86 fault sources: 9 strike-slip sources and 77 normal-slip sources. The longest fault source is *Castelluccio dei Sauri* (fault number (*id in Table 1)* 42, L = 93.2 km), and the shortest one is *Castrovillari* (*id* 63, L = 10.3 km). The mean length is 30 km. The dip angle values vary from 30° to 90°, and 70% of the fault sources have dip angles between 50° and 60°. The mean value of seismogenic thickness (ST) is approximately 12 km. The source with the largest ST is *Mattinata* (*id* 41, ST = 25 km), and the source with the thinnest ST is *Monte Santa Maria Tiberina* (*id* 9, ST = 2.5 km). Observed maximum magnitude (M_w) data have been assigned to 47 fault sources, and the values vary from 5.56 to 7.32. The fault source model is shown in Figure 3.

2.1.3 Expected seismicity rates

Each fault source is characterized by data, such as kinematics, geometry and slip rate, that we use as inputs for the FiSH code (Pace et al., 2016) to calculate the global budget of the seismic moment rate allowed by the structure based on predefined size-magnitude relationships, in terms of maximum magnitude (M_{max}) and the associated mean recurrence time (T_{mean}). Table 1 summarizes the geometric parameters used as FiSH input parameters for each fault source (seismogenic box) shown in Figure 3. For each source, up to five M_{max} values are computed (see the

Nat. Hazards Earth Syst. Sci. Discuss., doi:10.5194/nhess-2017-41, 2017
Manuscript under review for journal Nat. Hazards Earth Syst. Sci.
Published: 6 February 2017

example for Paganica fault source in Fig. 2b, details in Pace et al., 2016): a *MM0* value based on the calculated scalar seismic moment (M_0) and application of the standard formula $M_w = 2/3 (logM_0 – 9.1)$ (Hanks and Kanamori, 1979; IASPEI, 2005); two magnitude values using the Wells and Coppersmith (1994) empirical relationships for either the maximum subsurface rupture length (MRLD) and maximum rupture area (MRA); a value that corresponds to the maximum observed magnitude (MObs), if available; and a value (MASP, ASP for aspect ratio) computed by modifying the along-strike dimension if the rupture length exceeds the length predicted by the aspect ratio relationships (not in the case of Paganica in Fig. 2b), as derived by Peruzza and Pace (2002). Finally, to obtain the mean recurrence time of M_{max} (i.e., T_{mean}) we use the criterion of "segment seismic moment conservation" proposed by Field et al. (1999).

Once the fault source model and the calculated seismic moment rate, M_{max} (Fig. 2b) and T_{mean} are defined for each source, we compute the magnitude-frequency distributions of expected seismicity. For each fault source, we use two magnitude-frequency distributions: (i) a *CHaracteristic Gaussian* (*CHG*) model, a symmetric Gaussian bell curve centred on the M_{max} of each fault with a range of magnitudes equal to 1-sigma, and (ii) a *Truncated Gutenberg-Richter* (*TGR, Ordaz, 1999; Kagan, 2002*) model, with M_{max} as the upper threshold and M_w = 5.5 as the minimum threshold for all sources. In Figure 2c, we show an example of the expected seismicity rates in terms of the annual cumulative rates for the Paganica source, following the two above described magnitude-frequency distributions.

2.2 Distributed Source Model

Introducing distributed earthquakes into our PSH model is necessary because researchers have not been able to identify a causative source (i.e., a mapped fault) for a number of earthquakes in the historical catalogue. This lack of correlation between earthquakes and faults may be related to (i) interseismic strain accumulation in areas between major faults, (ii) earthquakes occurring on unknown or blind faults, (iii) earthquakes occurring on unmapped faults characterized by slip rates lower than the erosional processes, and/or (iv) the general lack of surface ruptures associated with faults generating M_w < 5.5 earthquakes.

Nat. Hazards Earth Syst. Sci. Discuss., doi:10.5194/nhess-2017-41, 2017
Manuscript under review for journal Nat. Hazards Earth Syst. Sci.
Published: 6 February 2017

Natural Hazards and Earth System Sciences
Open Access
EGU
Discussions

We used the historical catalogue of earthquakes (CPTI15; Rovida et al., 2016; Fig. 4) to model the occurrence of moderate-to-large (*M*w ≥ 4.5) earthquakes. The catalogue consists of 4,390 events and covers approximately the last one thousand years from 01/01/1005 to 28/12/2014. Before using the catalogue, we removed all events not considered the mainshock via a declustering filter (Gardner and Knopoff, 1977), resulting in a complete catalogue composed of 1,621 independent events. Moreover, to avoid any artificial effects related to double counting due to the use of two seismicity sources, i.e., the fault sources and the distributed seismicity sources, we removed events associated with known active faults from the CPTI15 earthquake catalogue. If the causative source of an earthquake is known, the impact of that earthquake does not need to be included in the seismicity smoothing process. The earthquake-source association has been made possible by neotectonics, palaeoseismology and seismotectonics papers (see supplement files) and, in a few cases, using macroseismic intensity maps. In Table 2, we listed the earthquakes with known causative fault sources. The differences in the smoothed rates given by eq. (1) using the complete and the modified catalogues are shown in Figure 5.

We apply the standard methodology developed by Frankel (1995) to estimate the density of seismicity on a grid with a latitude and longitude spacing of 0.05°. The smoothed rate of events in each cell *i* is determined as follows:

$$n_i = \frac{\Sigma_j n_j e^{\frac{-\Delta_{ij}^2}{c^2}}}{\Sigma_j e^{\frac{-\Delta_{ij}^2}{c^2}}} \qquad (1)$$

where *n* is the cumulative rate of earthquakes *ni* with magnitudes greater than the completeness magnitude Mc in each cell *i* of the grid and Δ*ij* is the distance between the centres of the grid cells *i* and *j*. The parameter *c* is the correlation distance. The sum is taken over cells *j* within a distance of 3*c* of cell *i*.

To compute earthquake rates, we adopted the completeness magnitude thresholds over different periods of time given by Stucchi et al. (2011) for five large zones (Fig. 4).

To optimize the smoothing distance Δ in eq. (1), we divided the earthquake catalogue into four 10-yr disjoint learning and target periods from the 1960s to the

Nat. Hazards Earth Syst. Sci. Discuss., doi:10.5194/nhess-2017-41, 2017
Manuscript under review for journal Nat. Hazards Earth Syst. Sci.
Published: 6 February 2017

1990s. For each pair of learning and target catalogues, we used the probability gain per earthquake to find the optimal smoothing distance (Kagan and Knopoff, 1977; Helmstetter et al., 2007). After assuming a spatially uniform earthquake density model as a reference model, the probability gain per earthquake G of a candidate model relative to a reference model is given by the following:

$$G = exp(\frac{L-L_0}{N}) \qquad (2)$$

where N is the number of events in the target catalogue, and L and L_0 are the joint log-likelihoods of the candidate model and the reference model, respectively. Under the assumption of a Poisson earthquake distribution, the joint log-likelihood of a model is given by the following:

$$L = \sum_{i_x=1}^{N_x} \sum_{j_y=1}^{N_y} log\ p\left[\lambda * (i_x, i_y), \omega\right] \qquad (3)$$

where p is the Poisson probability, λ is the spatial density, ω is the number of observed events during the target period, and the parameters *ix* and *jy* denote each corresponding longitude-latitude cell.

Figure 6 shows that, for the four different pairs of learning-target catalogues, the optimal smoothing distance *c* ranges from 30-40 km. Finally, the mean of all the probability gains per earthquake yields a maximum smoothing distance of 30 km (Fig. 6), which is then used in eq. (1).

The b-value of the Gutenberg-Richter distribution is calculated on a regional basis using the maximum-likelihood method of Weichert (1980), which allows multiple time periods with varying completeness levels to be combined. Following the approach recently proposed by Kamer and Hiemer (2015), we used a penalized likelihood-based method for the spatial estimation of Gutenberg-Richter's b-values based on the Voronoi tessellation of space. The Italian territory has been divided into a grid with a longitude/latitude spacing of 0.05°, and the centres of the grid cells represent the centres of Voronoi polygons. We vary the number of centres, Nv, from 3 to 50, generating 1000 tessellations for each Nv. The summed log-likelihood of each obtained tessellation is compared with the log-likelihood given by the simplest model (prior model) obtained using the whole earthquake dataset. We find that 673 random realizations performed better than the prior model. We calculate an ensemble model using these 673 solutions, and the mean b-value for each node of the grid is shown in Figure 4.

The maximum magnitude M_{max} assigned to each node of the grid, the nodal planes and the depths have been taken from the SHARE European project (Woessner et al., 2015). The SHARE project evaluated maximum magnitudes for large areas of Europe that depend on a joint procedure involving historical observations and tectonic regionalization. We adopted the lowest of the maximum magnitudes proposed by SHARE, but evaluating the impact of different maximum magnitudes is beyond the scope of this work.

Finally, the rates of expected seismicity for each node of the grid are assumed to follow the TGR model (Kagan 2002):

$$\lambda(M) = \lambda_0 \frac{\exp(-\beta M) - \exp(-\beta M_u)}{\exp(-\beta M_0) - \exp(-\beta M_u)} \qquad (4)$$

where the magnitude (M) is in the range M_0 (minimum magnitude) to M_u (upper or maximum magnitude), otherwise $\lambda(M)$ is 0, and where λ_0 is the smoothed rate of earthquakes at M_w = 4.5 and β = 2/3 b.

2.3 Combining Fault and Distributed Sources

Our PSH model requires the combination of the two source models related to the locations of expected seismicity rates into a single model. We introduced a distance-dependent linear weighting function, such that the contribution from the distributed sources linearly decreases from 1 to 0 with decreasing distance from the fault. The expected seismicity rates from the distributed sources model start at Mw = 4.5, which is lower than the minimum magnitude of the fault sources, and the weighting function acts only in the magnitude range overlapping the magnitude-frequency distribution of each fault. This weighting function is based on the assumption that faults tend to modify the surrounding deformation field (Fig. 7).

During fault system evolution, the increase in the size of a fault through linking with other faults results in an increase in displacement that is proportional to the quantity of strain accommodated by the fault (Kostrov, 1974). Under a constant regional strain rate, the activity of faults located across strike must eventually decrease (Nicol et al., 1997; Cowie, 1998; Roberts et al., 2004). Using analogue modelling, Mansfield and Cartwrigth (2001) have shown that faults grow via cycles of overlap, relay formation, breaching and linkage between neighbouring segments across a wide range of scales. During the evolution of a system, the merging of neighbour faults, mostly along strike, results in the formation of major faults, which accommodate the most displacement. These major faults are surrounded by minor faults, which accommodate lower degrees of displacement. To highlight the spatial pattern of major and minor faults, Figures 7a and 7b show sketches from the Mansfield and Cartwright (2001) experiment at two different stages: the approximate mid-point of the sequence and the end of the sequence. Numerical modelling performed by Cowie et al. (1993) has also shown similar evolutionary features for major and minor faults. The numerical fault simulation of Cowie et al. (1993) is able to reproduce the development of a normal fault system from the early nucleation stage to interaction with adjacent faults to full linkage and formation of a large through-going fault. The model also captures the increase in the displacement rate on the large linked fault. In Figures 7c and 7d, we focus on two stages of the simulation (from Cowie et al., 1993): the stage in which the fault segments have formed and some have become linked whilst others remain unlinked, and the last stage of the simulation.

Interestingly, the spatial distribution of major and minor faults are very similar in the experiments of both Mansfield and Cartwrigth (2001) and Cowie et al. (1993), as shown in Figures 7a-d. Developments during the early stage of major fault formation appear to control to the location and evolution of future faults, with areas where no major faults develop. The long-term evolution of a fault system is the consequence of the progressive cumulative effects of the slip histories, i.e., earthquake occurrences, of each fault. Earthquakes are generally thought to produce static and dynamic stress changes in the surrounding areas (King et al., 1994; Stein, 1999; Pace et al., 2014; Verdecchia and Carena, 2016). Static stress changes produce areas of negative stress in the hanging wall and footwall of a fault, also known as shadow zones, and positive stress zones located at the tip of the fault. The spatial distributions of decreases (unloading) and increases (loading) in stress during the long-term slip history of faults likely influence the distance along strike between major faults. Thus, given a known major active fault geometrically capable of hosting a $M_w \geq 5.5$ earthquake, the possibility that a future $M_w \geq 5.5$ earthquake will occur in the vicinity of the fault but is not caused by that fault should decrease as the distance

Nat. Hazards Earth Syst. Sci. Discuss., doi:10.5194/nhess-2017-41, 2017
Manuscript under review for journal Nat. Hazards Earth Syst. Sci.
Published: 6 February 2017

Natural Hazards and Earth System Sciences
Discussions
Open Access

from the fault decreases. On the other hand, earthquakes with magnitudes lower than 5.5 and those due to slip along minor faults are likely to occur everywhere within a fault system, including in proximity to a major fault.

In Figure 7e, we schematise the results from the analogue and numerical modelling of fault system evolution and indicated the area around major faults where it is unlikely for other major faults to develop. In Figure 7f, we show the next step in moving from geologic and structural considerations to source models for fault sources and distributed seismicity to serve as inputs for the PSH model. Fault sources are used to model major faults and are represented by a master fault (i.e., one or more major faults) and its projection at the surface. Distributed seismicity is used to model seismicity occurring on minor, unknown or unmapped faults. Depending on the position of a distributed seismicity point with respect to the buffer zone around major faults, the rates of expected distributed seismicity are left unmodified, reduced or zero.

Specifically, we introduced a slip rate and a distance-weighting function based on the above reasoning. The probability of the occurrence of an earthquake (Pe) with a Mw greater than or equal to the minimum magnitude of the fault is as follows:

$$Pe = 0, \text{ when } d \leq 1 \text{ km}; \qquad Pe = 1/d, \text{ when } d > 1 \text{ km} \qquad (5)$$

where d is the Joyner-Boore distance from a fault source. The maximum value for d (d_{max}) is controlled by the slip rate of the fault. For faults with slip rates of ≥ 1 mm/yr, we assumed d_{max} = L/2 (L is the length along strike, Fig. 2a); for faults with slip rates of 0.3 - 1 mm/yr, d_{max} = L/3; and for faults with slip rates of ≤ 0.3 mm/yr, d_{max} = L/4. We applied eq. (5) to the smoothed occurrence rates of the distributed seismogenic sources. Because we used two models of the magnitude-frequency distribution of fault sources, i.e., the TGR and CHG models, we also calculated two rates of expected seismicity for the distributed seismogenic sources. These two distributed seismogenic source models differ because the minimum magnitude of the faults is Mw 5.5 in the TGR model but depends on each fault source dimension in the CHG model.

Our approach allows incompleteness in the fault database to be bypassed, which is advantageous because all fault databases should be considered incomplete. In our approach, the seismicity is modified only in the vicinity of mapped faults. The remaining areas are fully described by the *distributed* model. With this approach, we do not define areas with reliable fault information, and the locations of currently unknown faults can be easily included when they are discovered in future.

3. Results and Discussion

To obtain PSH maps designed under the traditional Poisson hypothesis, we assign the calculated expected seismicity rates, as described in previous sections, to their pertinent geometries, i.e., individual 3D seismogenic sources for the *fault model* and point sources for the *distributed model*. All the computations are performed using the well-known OpenQuake Engine (GEM, 2016) with a grid spacing of 0.05° in both latitude and longitude. The ground motion prediction equations (GMPE) of Akkar et al. (2013), Chiou et al., (2008), Faccioli et al., (2010) and Zhao et al., (2006) are used, as suggested by the SHARE European project (Woessner et al., 2015). In addition, we also used Bindi et al. 2014, a GMPE calibrated using Italian data. We put together all GMPE in a logic tree with the same weight of 0.2 for each branch. The distances used for each GMPE are the Joyner and Boore distance for Akkar 2013, Bindi 2014 and Chiou 2008 and the closest rupture distance for Faccioli 2010 and Zaho 2006.

The results of the fault source model, distributed source model, and the aggregated model are expressed in terms of peak ground acceleration (PGA) for exceedance probabilities of 10% and 2% in 50 years, corresponding to return periods of 475 and 2,475 years, respectively (Fig. 8).

To explore the epistemic uncertainty due to the distribution of activity rates over the range of magnitudes in the fault source model, we compared the seismic hazard levels estimated by the TGR and CHG fault source models (left column in Fig. 8) using the TGR and CHG magnitude-frequency distributions for all the fault sources (details in par. 2.1.3). Although both models have the same amount of seismic moment release, the different magnitude-frequency distributions generate clear differences. In fact, in the *TGR* model, all faults exhibit a 10% probability of exceedance in 50 years in the hazard maps, whereas in the *CHG* model, only a few faults located in the central Apennines and Calabria contribute to the seismic hazard. This difference is due to the different shapes of the magnitude-frequency

Nat. Hazards Earth Syst. Sci. Discuss., doi:10.5194/nhess-2017-41, 2017
Manuscript under review for journal Nat. Hazards Earth Syst. Sci.
Published: 6 February 2017

Natural Hazards and Earth System Sciences
Open Access
Discussions

distributions in the two models (Fig. 2c). The rates of earthquakes with magnitudes between 5.5 and approximately 6, which are likely the main contributors to these levels of seismic hazard, are generally higher in the *TGR* model than in the *CHG* model. At a 2% probability of exceedance in 50 years, all fault sources in the CHG contribute to the seismic hazard, but the absolute values are still generally higher in the *TGR* model.

The *distributed model* (central column in Fig. 8) depicts a more uniform shape of the seismic hazard than the fault source models. A PGA threshold of 0.125 g at a 10% probability of exceedance in 50 years and a threshold of 0.225 g at a 2% probability of exceedance in 50 years envelope a large part of peninsular Italy and Sicily. Two areas with higher seismic hazard levels are located in the central Apennines and north-eastern Sicily.

The total model, obtained by combining the fault and distributed source models, is shown in the right column of Figure 8. Areas with comparatively high seismic hazard levels, i.e., hazard levels greater than 0.225 g and greater than 0.45 g at 50-yr exceedance probabilities of 10% and 2%, respectively, are located throughout the Apennines, in Calabria and in Sicily. The fault source models contribute to the total seismic hazard in the Apennines, Calabria and eastern Sicily, where the highest PGA values are observed.

Figure 9 shows the contributions to the total seismic hazard by the *fault* and *distributed* source models at a specific site (L'Aquila, 42.400-13.400). Interestingly, in Figure 9, the *distributed* source dominates the seismic hazard for exceedance probabilities greater than ~81% in 50 years, but the contribution of *fault* sources cannot be neglected. Conversely, at exceedance probabilities of less than ~10% in 50 years, the total hazard is mainly to completely obtained by the *fault* source model.

Figure 10 shows seismic hazard maps with PGAs at 10% and 2% exceedance probabilities in 50 years for the *fault* sources, *distributed* sources and a combination of the two. These data were obtained by applying a magnitude-frequency distribution to each fault (as shown in Figure 3). The results from this model, called the *Mixed* model, therefore have values between those of the two end-members shown in Figure 8. The choice of the appropriate magnitude-frequency distribution for a fault source is a difficult task because palaeoseismological studies are scarce and it is often difficult to establish clear relationships between faults and observed seismicity. If an earthquake assigned to a fault source (see Table 2 for earthquake-source associations) has a magnitude lower or higher than the bell curve of the *CHG* model distribution, the *TGR* model is applied to that fault source. Otherwise, the *CHG* model, peaking at the calculated M_{max}, is applied. Of course, errors in this approach can originate from a misallocation of historical earthquakes, and we also cannot exclude the possibility that potentially active faults responsible for historical earthquakes have been not yet mapped. The magnitude-frequency distribution assigned to each fault source in our *Mixed* model is shown in Figure 3.

Figure 11 shows the *CHG*, *TGR* and *Mixed* model hazard curves for three sites (Cesena, L'Aquila and Crotone, Fig. 12c). As previously mentioned, the results of the Mixed model, due to the construction of the model, are between those of the *CHG* and *TGR* models. The relative positions of the hazard curves derived from the two end-member models and the Mixed model depend on the number of nearby fault sources that have been modelled using a magnitude-frequency distribution and on the distance of the site from the faults. For example, in the case of the Crotone site, the majority of the fault sources in the Mixed model have been modelled using a CHG magnitude-frequency distribution. Thus, the resulting hazard curve is close to the *CHG* model. For the Cesena site, the three hazard curves overlap. Because the distance between Cesena and the closest fault sources is approximately 60 km, the impact of the fault model is less than the impact of the *distributed* source model. In this case, the choice of a particular magnitude-frequency distribution could have a limited impact on the modelling of the *distributed* sources. Notably, for an annual frequency of exceedance (*AFOE*) lower than 10^{-4}, the *TGR fault* source model values are generally higher than those the *CHG*, and the three models converge at *AFOE* < 10^{-4}. The resulting seismic hazard estimates depend on the assumed seismicity rate model (*TGR* vs. *CHG*), especially for intermediate magnitude events (5.5 to ~6.5). Because we assume that the maximum magnitude is imposed by the fault geometry and that the seismic moment release is controlled by the slip rate, the *TGR* model leads to the highest hazard values because this range of magnitude contributes the most to the hazard level.

In Figure 12, we investigated the influences of the Mixed *fault* source model and the Mixed *distributed* source model on the total hazard for the whole study area and the variability in the hazard results. The maps in Figure 12a show that the contribution to the total hazard from the *fault* model generally decrease with increases in the exceedance probability from 2% to 81% in 50 years. At a 2% probability of exceedance in 50 years, the total hazard in the Apennines and in eastern Sicily is mainly related to faults, whereas at an 81% probability of exceedance in 50 years, the contributions of the *fault* model are high in local areas in central Italy and southern Calabria.

Moreover, we examined the contributions of the *fault* and *distributed* sources along three E-W-oriented profiles in northern, central and southern Italy (Fig. 12b). In areas with faults, the hazard estimated by the fault model is generally higher than that estimated by the corresponding *distributed* source model. Notable exceptions are present in areas proximal to slower slipping active faults at an 81% probability of exceedance in 50 years (profile A), at the eastern and western boundaries of the faulted area in central Italy (profile B), and in the area where the contribution of the *distributed* source model is equal to that of the *fault* model at a 10% probability of exceedance in 50 years (eastern part of profile C).

The features depicted by the three profiles result from a combination of slip rates and spatial distribution of faults in the *fault* source model. This pattern should be considered a critical aspect of using fault models for PSH analysis. In fact, the proposed approach requires a high level of expertise in active tectonics and cautious expert judgement at many levels of procedure. First, the seismic hazard estimate is based on the definition of a segmentation model, which requires a series of rules based on observations and empirical regression between earthquakes and the size of the causative fault. New data might make it necessary to revise the rules or reconsider the role of the segmentation. In some cases, expert judgement could permit discrimination among different fault source models. Alternatively, all models should be considered branches in a logic tree approach.

We finally propose a fault seismicity model in which the magnitude-frequency distribution of each fault source has been chosen based on an analysis of the occurrences of earthquakes that can be tentatively or confidently assigned to a certain fault. To describe the fault activity, we applied a probability density function to the magnitude, as commonly performed in the literature: the TGR model and the characteristic maximum magnitude model, which consists of a truncated normal distribution centred on the maximum magnitude. Other magnitude-frequency distributions have been proposed to model the earthquake recurrence for a fault. For example, Youngs and Coppersmith (1985) proposed adjusting the truncated exponential model to allow for the increased likelihood of characteristic events. However, we focused only on two models, as we believe that, instead of a “blind” or qualitative characterization of the magnitude-frequency distribution of a fault source, future applications of statistical tests to the compatibility between expected earthquake rates and observed historical seismicity could be used as an objective way to identify the best expected seismicity magnitude-frequency distribution.

To focus on the general procedure for spatially integrating faults with sources representing distributed (or off-fault) seismicity, we did not investigate the impact of other smoothing procedures on the distributed sources, and we used fixed kernels with a constant bandwidth (as in the works of Kagan and Jackson, 1994; Frankel et al. 1997; Zechar and Jordan, 2010). The testing of adaptive bandwidths (e.g., Stock and Smith, 2002; Helmstetter et al., 2006, 2007; Werner et al., 2011) or weighted combinations of both models has been reserved for future implementations.

The strength of our approach is the possibility of integrating different levels of information on the active faults in Italy, but the final result is unavoidably linked to the quality of the databases. Our work focused on presenting and applying a new approach for evaluating seismic hazards based on active faults and intentionally avoided the introduction of uncertainties due to the use of different segmentation rules or other slip rate values for faults. Moreover, the impact of ground motion predictive models is certainly important in seismic hazard assessment but beyond the scope of this work. Future steps will be devoted to analysing these uncertainties and evaluating their impacts on the seismic hazard estimate.

4. Conclusions

Nat. Hazards Earth Syst. Sci. Discuss., doi:10.5194/nhess-2017-41, 2017
Manuscript under review for journal Nat. Hazards Earth Syst. Sci.
Published: 6 February 2017

We presented our first national-scale PSH model for Italy, which summarizes and integrates the fault-based PSH models developed since the work of Pace et al. (2006).

The model proposed here combines a fault source model based on over 110 faults with 86 fault sources and a distributed source model. For each fault source, the maximum magnitude and its uncertainty has been derived by applying scaling relationships, and the rates of seismic activity have been derived by applying slip rates to seismic moment evaluations and balancing this seismic moment over two magnitude-frequency distributions.

To account for unknown faults, a distributed seismicity model has also been applied following the well-known Frankel (1995) methodology for the calculation of seismicity parameters.

The fault sources and distributed sources have been integrated via a new approach based on the idea that deformation in the vicinity of an active fault is concentrated along the fault and that the seismic activity in the surrounding region is reduced. In particular, a distance-dependent linear weighting function has been introduced to allow the contribution from the distributed sources (in the magnitude range overlapping the magnitude-frequency distribution of each fault source) to linearly decrease from 1 to 0 with decreasing distance from a fault. The strength of our approach lies in the ability to integrate the different levels of available information for active faults that actually exist in Italy (or elsewhere), but the final result is unavoidably linked to the quality of the databases.

The probabilistic seismic hazard maps produced using our model show a hazard pattern similar to that of the current national maps at the national scale, but some significant differences in hazard are present at the regional-to-local scale.

The impact on the hazard maps of using different magnitude-frequency distributions to derive seismic activity rates has been investigated. The PGA values in the hazard maps generated by the *TGR* model are higher than those in the hazard maps generated by *CHG* model. This difference is because the rates of earthquakes with magnitudes from 5.5 to approximately 6 are generally higher in the *TGR* model than in the *CHG* model. Moreover, the relative contributions of fault source models and distributed source models have been identified in maps and profiles in three sectors of the study area. These profiles show that: the hazard is generally higher where faults have been used; and for high values of probability of exceedance the contribution of the *distributed* sources equal the *fault* model one.

Finally, a preferred model, called the *Mixed* model, was obtained by applying a magnitude-frequency distribution to each fault. All data, including the locations and parameters of fault sources, are provided in the Supplements of this paper.

This new PSH model is not intended to replace, integrate or test the currently official national seismic hazard model for Italy. While some aspects remain to be implemented in our approach (e.g., the integration of reverse/thrust faults in the database, sensitivity tests for the distance-dependent linear weighting function parameters, sensitivity tests for possible different segmentation models, and fault source models that account for fault interaction), the proposed model represents an advance in terms of input data (quantity and quality) and methodology based on a decade of research in the field of fault-based approaches to regional seismic hazard modelling.

References

Akinci, A., Galadini, F., Pantosti, D., Petersen, M., Malagnini, L., and Perkins, D.: Effect of Time Dependence on Probabilistic Seismic-Hazard Maps and Deaggregation for the Central Apennines, Italy, B Seismol Soc Am, 99, 585-610, 2009.

Akkar, S., Sandikkaya, M.A. , Bommer, J.J.: Empirical Ground-Motion Models for Point and Extended-Source Crustal Earthquake Scenarios in Europe and the Middle East, Bulletin of Earthquake Engineering, ISSN:1570-761X, 2013.

Benedetti, L., Manighetti, I., Gaudemer, Y., Finkel, R., Malavieille, J., Pou, K., Arnold, M., Aumaitre, G., Bourles, D., and Keddadouche, K.: Earthquake synchrony and clustering on Fucino faults (Central Italy) as revealed from in situ Cl-36 exposure dating, J Geophys Res-Sol Ea, 118, 4948-4974, 2013.

Bindi, D., Massa, M., Luzi, L., Ameri, G., Pacor, F., Puglia, R., and Augliera, P.: Pan-European ground-motion prediction equations for the average horizontal component of PGA, PGV, and 5%-damped PSA at spectral periods up to 3.0 s using the RESORCE dataset (vol 12, pg 391, 2014), B Earthq Eng, 12, 431-448, 2014.

Boncio, P., Lavecchia, G., and Pace, B.: Defining a model of 3D seismogenic sources for Seismic Hazard Assessment applications: The case of central Apennines (Italy), J Seismol, 8, 407-425, 2004.

Boncio, P., Pizzi, A., Cavuoto, G., Mancini, M., Piacentini, T., Miccadei, E., Cavinato, G. P., Piscitelli, S., Giocoli, A., Ferretti, G., De Ferrari, R., Gallipoli, M. R., Mucciarelli, M., Di Fiore, V., Franceschini, A., Pergalani, F., Naso, G., and Macroarea, W. G.: Geological and geophysical characterisation of the Paganica - San Gregorio area after the April 6, 2009 L'Aquila earthquake (M-w 6.3, central Italy): implications for site response, B Geofis Teor Appl, 52, 491-512, 2011.

Bull, J. M., Barnes, P. M., Lamarche, G., Sanderson, D. J., Cowie, P. A., Taylor, S. K., and Dix, J. K.: High-resolution record of displacement accumulation on an active normal fault: implications for models of slip accumulation during repeated earthquakes, J Struct Geol, 28, 1146-1166, 2006.

Chiou, B. S. J. and Youngs, R. R.: An NGA model for the average horizontal component of peak ground motion and response spectra, Earthq Spectra, 24, 173-215, 2008.

Cornell, C.A.: Engineering seismic risk analysis, Bull. Seism. Soc. Am., 58,1583-1606, 1968.

Cowie, P. A.: A healing-reloading feedback control on the growth rate of seismogenic faults, J Struct Geol, 20, 1075-1087, 1998.

Cowie, P. A., Roberts, G. P., Bull, J. M., and Visini, F.: Relationships between fault geometry, slip rate variability and earthquake recurrence in extensional settings, Geophys J Int, 189, 143-160, 2012.

Cowie, P. A., Underhill, J. R., Behn, M. D., Lin, J., and Gill, C. E.: Spatio-temporal evolution of strain accumulation derived from multi-scale observations of Late Jurassic rifting in the northern North Sea: A critical test of models for lithospheric extension, Earth Planet Sc Lett, 234, 401-419, 2005.

Nat. Hazards Earth Syst. Sci. Discuss., doi:10.5194/nhess-2017-41, 2017
Manuscript under review for journal Nat. Hazards Earth Syst. Sci.
Published: 6 February 2017

Cowie, P. A., Vanneste, C., and Sornette, D.: Statistical Physics Model for the Spatiotemporal Evolution of Faults, J Geophys Res-Sol Ea, 98, 21809-21821, 1993.

Faccioli, E., Bianchini, A., and Villani, M.: New ground motion prediction equations for t > 1 s and their influence on seismic hazard assessment, In: Proceedings of the University of Tokyo symposium on long-period ground motion and urban disaster mitigation, 2010.

Ferranti, L., Palano, M., Cannavo, F., Mazzella, M. E., Oldow, J. S., Gueguen, E., Mattia, M., and Monaco, C.: Rates of geodetic deformation across active faults in southern Italy, Tectonophysics, 621, 101-122, 2014.

Field, E. H., Biasi, G. P., Bird, P., Dawson, T. E., Felzer, K. R., Jackson, D. D., Johnson, K. M., Jordan, T. H., Madden, C., Michael, A. J., Milner, K. R., Page, M. T., Parsons, T., Powers, P. M., Shaw, B. E., Thatcher, W. R., Weldon, R. J., and Zeng, Y. H.: Long-Term Time-Dependent Probabilities for the Third Uniform California Earthquake Rupture Forecast (UCERF3), B Seismol Soc Am, 105, 511-543, 2015.

Field, E. H., Jackson, D. D., and Dolan, J. F.: A mutually consistent seismic-hazard source model for southern California, B Seismol Soc Am, 89, 559-578, 1999.

Finnegan, N. J., Schumer, R., and Finnegan, S.: A signature of transience in bedrock river incision rates over timescales of 10(4)-10(7) years, Nature, 505, 391-+, 2014.

Frankel, A.: Simulating Strong Motions of Large Earthquakes Using Recordings of Small Earthquakes - the Loma-Prieta Mainshock as a Test-Case, B Seismol Soc Am, 85, 1144-1160, 1995.

Frankel, A., Mueller, C., Barnhard, T., Perkins, D., Leyendecker, E. V., Dickman, N., Hanson, S.. and Hopper, M.: Seismic-hazard maps for California, Nevada, and Western Arizona/Utah', U.S. Geological Survey Open-File Rept. 97-130, 1997.

Gallen, S. F., Pazzaglia, F. J., Wegmann, K. W., Pederson, J. L., and Gardner, T. W.: The dynamic reference frame of rivers and apparent transience in incision rates, Geology, 43, 623-626, 2015.

Garcia-Mayordomo, J., Gaspar-Escribano, J. M., and Benito, B.: Seismic hazard assessment of the Province of Murcia (SE Spain): analysis of source contribution to hazard, J Seismol, 11, 453-471, 2007.

Nat. Hazards Earth Syst. Sci. Discuss., doi:10.5194/nhess-2017-41, 2017
Manuscript under review for journal Nat. Hazards Earth Syst. Sci.
Published: 6 February 2017

Gardner, J. K., Knopoff, L.: Is the sequence of earthquakes in Southern California, with aftershocks removed, Poissonian?'. Bulletin of the Seismological Society of America, 64, 1363-1367, 1974.

Gardner, T. W., Jorgensen, D. W., Shuman, C., and Lemieux, C. R.: Geomorphic and Tectonic Process Rates - Effects of Measured Time Interval, Geology, 15, 259-261, 1987.

GEM: The OpenQuake-engine User Manual. Global Earthquake Model (GEM) Technical Report, doi: 10.13117/GEM.OPENQUAKE.MAN.ENGINE.1.9/01, 189 pages, 2016.

Gunderson, K. L., Anastasio, D. J., Pazzaglia, F. J., and Picotti, V.: Fault slip rate variability on 10(4)-10(5)yr timescales for the Salsomaggiore blind thrust fault, Northern Apennines, Italy, Tectonophysics, 608, 356-365, 2013.

Hanks, T. C., and Kanamori, H.: A moment magnitude scale, Journal of Geophysics Research, 84, 2348–2350, 1979.

Helmstetter, A., Kagan, Y. Y., and Jackson, D. D.: Comparison of short-term and time-independent earthquake forecast models for southern California, B Seismol Soc Am, 96, 90-106, 2006.

Helmstetter, A., Kagan, Y. Y., and Jackson, D. D.: High-resolution time-independent grid-based forecast for M <= 5 earthquakes in California, Seismol Res Lett, 78, 78-86, 2007.

International Association of Seismology and Physics of the Earth's Interior (IASPEI): Summary of Magnitude Working Group recommendations on standard procedures for determining earthquake magnitudes from digital data, http://www.iaspei.org/ commissions/CSOI/summary_of_WG_recommendations_2005.pdf (last accessed December 2015), 2005.

Kagan, Y. Y.: Seismic moment distribution revisited: I. Statistical results, Geophys J Int, 148, 520-541, 2002.

Kagan, Y., and Knopoff, L.: Earthquake risk prediction as a stochastic process, Physics of the Earth and Planetary Interiors, 14, 97–108, 1977.

Kagan, Y. Y. and Jackson, D. D.: Long-Term Probabilistic Forecasting of Earthquakes, J Geophys Res-Sol Ea, 99, 13685-13700, 1994.

Nat. Hazards Earth Syst. Sci. Discuss., doi:10.5194/nhess-2017-41, 2017
Manuscript under review for journal Nat. Hazards Earth Syst. Sci.
Published: 6 February 2017

Natural Hazards and Earth System Sciences
Open Access
Discussions

Kamer, Y. and Hiemer, S.: Data-driven spatial b value estimation with applications to California seismicity: To b or not to b, J Geophys Res-Sol Ea, 120, 5191-5214, 2015.

King, G. C. P., Stein, R. S., and Lin, J.: Static Stress Changes and the Triggering of Earthquakes, B Seismol Soc Am, 84, 935-953, 1994.

Kostrov, V. V.: Seismic moment and energy of earthquakes, and seismic flow of rock, Physic of the Solid Earth, 1, 23-44, 1974.

Main, I.: Statistical physics, seismogenesis, and seismic hazard, Rev Geophys, 34, 433-462, 1996.

Mansfield, C. and Cartwright, J.: Fault growth by linkage: observations and implications from analogue models, J Struct Geol, 23, 745-763, 2001.

Meletti, C., Visini, F., D'Amico, V., and Rovida A.: Seismic hazard in central Italy and the 2016 Amatrice earthquake, Annals of Geophysics, 59, doi:10.4401/ag-7248, 2016.

McClymont, A. F., Villamor, P., and Green, A. G.: Assessing the contribution of off-fault deformation to slip-rate estimates within the Taupo Rift, New Zealand, using 3-D ground-penetrating radar surveying and trenching, Terra Nova, 21, 446-451, 2009a.

McClymont, A. F., Villamor, P., and Green, A. G.: Fault displacement accumulation and slip rate variability within the Taupo Rift (New Zealand) based on trench and 3-D ground-penetrating radar data, Tectonics, 28, 2009b.

Nicol, A., Walsh, J., Berryman, K., and Villamor, P.: Interdependence of fault displacement rates and paleoearthquakes in an active rift, Geology, 34, 865-868, 2006.

Nicol, A., Walsh, J., Mouslopoulou, V., and Villamor, P.: Earthquake histories and Holocene acceleration of fault displacement rates, Geology, 37, 911-914, 2009.

Nicol, A., Walsh, J. J., Villamor, P., Seebeck, H., and Berryman, K. R.: Normal fault interactions, paleoearthquakes and growth in an active rift, J Struct Geol, 32, 1101-1113, 2010.

Nicol, A., Walsh, J. J., Watterson, J., and Underhill, J. R.: Displacement rates of normal faults, Nature, 390, 157-159, 1997.

Ordaz, M. and Reyes, C.: Earthquake hazard in Mexico City: Observations versus computations, B Seismol Soc Am, 89, 1379-1383, 1999.

Nat. Hazards Earth Syst. Sci. Discuss., doi:10.5194/nhess-2017-41, 2017
Manuscript under review for journal Nat. Hazards Earth Syst. Sci.
Published: 6 February 2017

Pace, B., Bocchini, G. M., and Boncio, P.: Do static stress changes of a moderate-magnitude earthquake significantly modify the regional seismic hazard? Hints from the L'Aquila 2009 normal-faulting earthquake (Mw 6.3, central Italy), Terra Nova, 26, 430-439, 2014.

Pace, B., Peruzza, L., Lavecchia, G., and Boncio, P.: Layered seismogenic source model and probabilistic seismic-hazard analyses in central Italy, B Seismol Soc Am, 96, 107-132, 2006.

Pace, B., Visini, F., and Peruzza, L.: FiSH: MATLAB Tools to Turn Fault Data into Seismic-Hazard Models, Seismol Res Lett, 87, 374-386, 2016.

Peruzza, L., and Pace B.: Sensitivity analysis for seismic source characteristics to probabilistic seismic hazard assessment in central Apennines (Abruzzo area), Bollettino di Geofisica Teorica ed Applicata 43, 79–100, 2002.

Peruzza, L., Pace, B., and Visini, F.: Fault-Based Earthquake Rupture Forecast in Central Italy: Remarks after the L'Aquila M-w 6.3 Event, B Seismol Soc Am, 101, 404-412, 2011.

Peruzza, L., Gee, R., Pace, B., Roberts, G., Scotti, O., Visini,F., Benedetti, L., and Pagani, M.: PSHA after a strong earthquake: hints for the recovery, Annals of Geophysics, 59, doi:10.4401/ag-7257, 2016

Roberts, G. P., Cowie, P., Papanikolaou, I., and Michetti, A. M.: Fault scaling relationships, deformation rates and seismic hazards: an example from the Lazio-Abruzzo Apennines, central Italy, J Struct Geol, 26, 377-398, 2004.

Roberts, G. P. and Michetti, A. M.: Spatial and temporal variations in growth rates along active normal fault systems: an example from The Lazio-Abruzzo Apennines, central Italy, J Struct Geol, 26, 339-376, 2004.

Robinson, R., Nicol, A., Walsh, J. J., and Villamor, P.: Features of earthquake occurrence in a complex normal fault network: Results from a synthetic seismicity model of the Taupo Rift, New Zealand, J Geophys Res-Sol Ea, 114, 2009.

Rovida, A., Locati, M., Camassi, R., Lolli, B., and Gasperini P.: CPTI15, the 2015 version of the Parametric Catalogue of Italian Earthquakes. Istituto Nazionale di Geofisica e Vulcanologia. doi:http://doi.org/10.6092/INGV.IT-CPTI15, 2016.

Scotti, O., Clement, C., and Baumont, D.: Seismic hazard for design and verification of nuclear installations in France: regulatory context, debated issues and ongoing developments, B Geofis Teor Appl, 55, 135-148, 2014.

Stein, R. S., King, G. C. P., and Lin, J.: Stress Triggering of the 1994 M=6.7 Northridge, California, Earthquake by Its Predecessors, Science, 265, 1432-1435, 1994.

Stirling, M., McVerry, G., Gerstenberger, M., Litchfield, N., Van Dissen, R., Berryman, K., Barnes, P., Wallace, L., Villamor, P., Langridge, R., Lamarche, G., Nodder, S., Reyners, M., Bradley, B., Rhoades, D., Smith, W., Nicol, A., Pettinga, J., Clark, K., and Jacobs, K.: National Seismic Hazard Model for New Zealand: 2010 Update, B Seismol Soc Am, 102, 1514-1542, 2012.

Stock, C. and Smith, E. G. C.: Adaptive kernel estimation and continuous probability representation of historical earthquake catalogs, B Seismol Soc Am, 92, 904-912, 2002a.

Stock, C. and Smith, E. G. C.: Comparison of seismicity models generated by different kernel estimations, B Seismol Soc Am, 92, 913-922, 2002b.

Stucchi, M., Meletti, C., Montaldo, V., Crowley, H., Calvi, G. M., and Boschi, E.: Seismic Hazard Assessment (2003-2009) for the Italian Building Code, B Seismol Soc Am, 101, 1885-1911, 2011.

Verdecchia, A. and Carena, S.: Coulomb stress evolution in a diffuse plate boundary: 1400 years of earthquakes in eastern California and western Nevada, USA, Tectonics, 35, 1793-1811, 2016.

Visini, F. and Pace, B.: Insights on a Key Parameter of Earthquake Forecasting, the Coefficient of Variation of the Recurrence Time, Using a Simple Earthquake Simulator, Seismol Res Lett, 85, 703-713, 2014.

Weichert, D. H: Estimation of the earthquake recurrence parameters for unequal observation periods for different magnitudes, Bulletin of the Seismological Society of America, 70, 1337-1346, 1980.

Wells, D. L. and Coppersmith, K. J.: New Empirical Relationships among Magnitude, Rupture Length, Rupture Width, Rupture Area, and Surface Displacement, B Seismol Soc Am, 84, 974-1002, 1994.

Werner, M. J., Helmstetter, A., Jackson, D. D., Kagan, Y. Y., and Wiemer, S.: Adaptively smoothed seismicity earthquake forecasts for Italy, Ann Geophys-Italy, 53, 107-116, 2010.

Woessner, J., Laurentiu, D., Giardini, D., Crowley, H., Cotton, F., Grunthal, G., Valensise, G., Arvidsson, R., Basili, R., Demircioglu, M. B., Hiemer, S., Meletti, C., Musson, R. W., Rovida, A. N., Sesetyan, K., Stucchi, M., and

Consortium, S.: The 2013 European Seismic Hazard Model: key components and results, B Earthq Eng, 13, 3553-3596, 2015.

Youngs, R. R. and Coppersmith, K. J.: Implications of Fault Slip Rates and Earthquake Recurrence Models to Probabilistic Seismic Hazard Estimates, B Seismol Soc Am, 75, 939-964, 1985.

Zechar, J. D. and Jordan, T. H.: Simple smoothed seismicity earthquake forecasts for Italy, Ann Geophys-Italy, 53, 99-105, 2010.

Zhao, J. X., Zhang, J., Asano, A., Ohno, Y., Oouchi, T., Takahashi, T., Ogawa, H., Irikura, K., Thio, H. K., Somerville, P. G., Fukushima, Y., and Fukushima, Y.: Attenuation relations of strong ground motion in Japan using site classification based on predominant period, B Seismol Soc Am, 96, 898-913, 2006.

Nat. Hazards Earth Syst. Sci. Discuss., doi:10.5194/nhess-2017-41, 2017
Manuscript under review for journal Nat. Hazards Earth Syst. Sci.
Published: 6 February 2017

Natural Hazards and Earth System Sciences
Open Access
Discussions

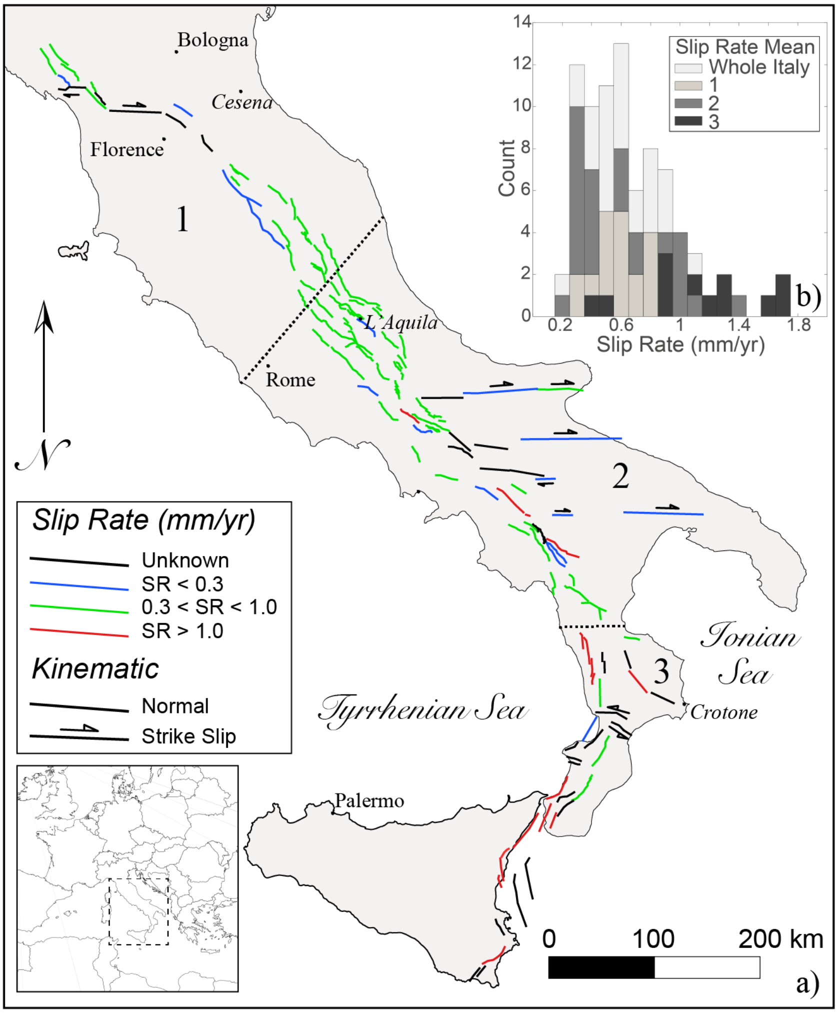

Fig. 1 a) Map of normal and strike-slip active faults used in this study. Colour scale indicates slip rate. b) Histogram of slip rate distribution for the whole study area and for three sub-sectors. The numbers 1, 2 and 3 are for the Northern Apennines, Central-Southern Apennines and Calabria-Sicilian coast regions, respectively. The dotted black lines are the boundaries of the regions.

Nat. Hazards Earth Syst. Sci. Discuss., doi:10.5194/nhess-2017-41, 2017
Manuscript under review for journal Nat. Hazards Earth Syst. Sci.
Published: 6 February 2017

Natural Hazards and Earth System Sciences
Open Access
Discussions

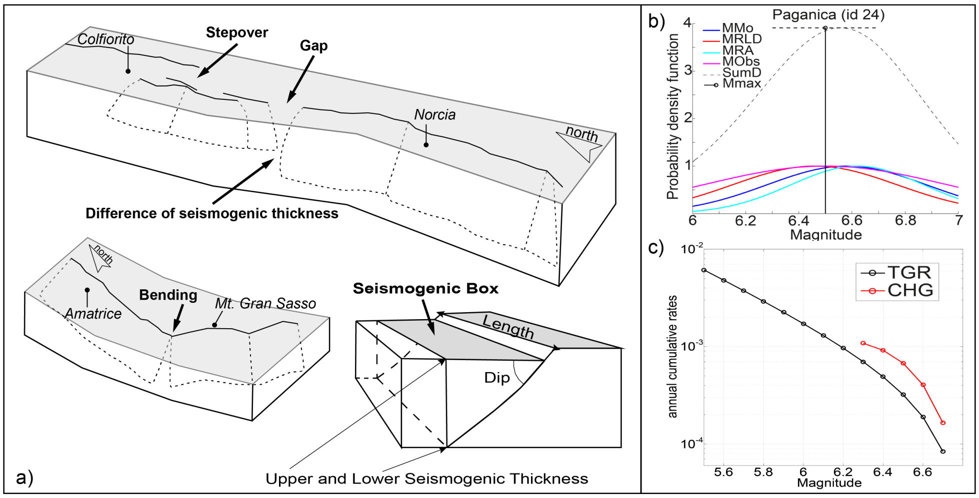

Fig. 2 a) Conceptual model of active faults and segmentation rules adopted to define a fault source and its planar projection, forming a seismogenic box [modified by Boncio et al., 2004]. b) Example of FiSH code output (see Pace et al., 2016 for details) for the Paganica fault source, showing the combination of magnitude estimates from empirical relationships and observations, both of which are affected by uncertainties. In this example, four magnitudes are estimated: MMo (blue line) is from the standard formula (IASPEI, 2005); the maximum subsurface fault length (MRLD, red line) and maximum rupture area (MRA, cyan line) are from the empirical relationships of Wells and Coppersmith (1994) for length and area, respectively; and Mobs (magenta line) is the largest observed moment magnitude. The black dashed line represents the summed probability density curve (SumD), the vertical black line represents the central value of the Gaussian fit of the summed probability density curve (Mmax), and the horizontal black dashed line represents its standard deviation (σMmax). The input values that were used to obtain this output are provided in Table 1. c) Comparison of the magnitude–frequency distributions for the Paganica source, which were obtained using the CHG model (red line) and the TGR model (black line).

Nat. Hazards Earth Syst. Sci. Discuss., doi:10.5194/nhess-2017-41, 2017
Manuscript under review for journal Nat. Hazards Earth Syst. Sci.
Published: 6 February 2017

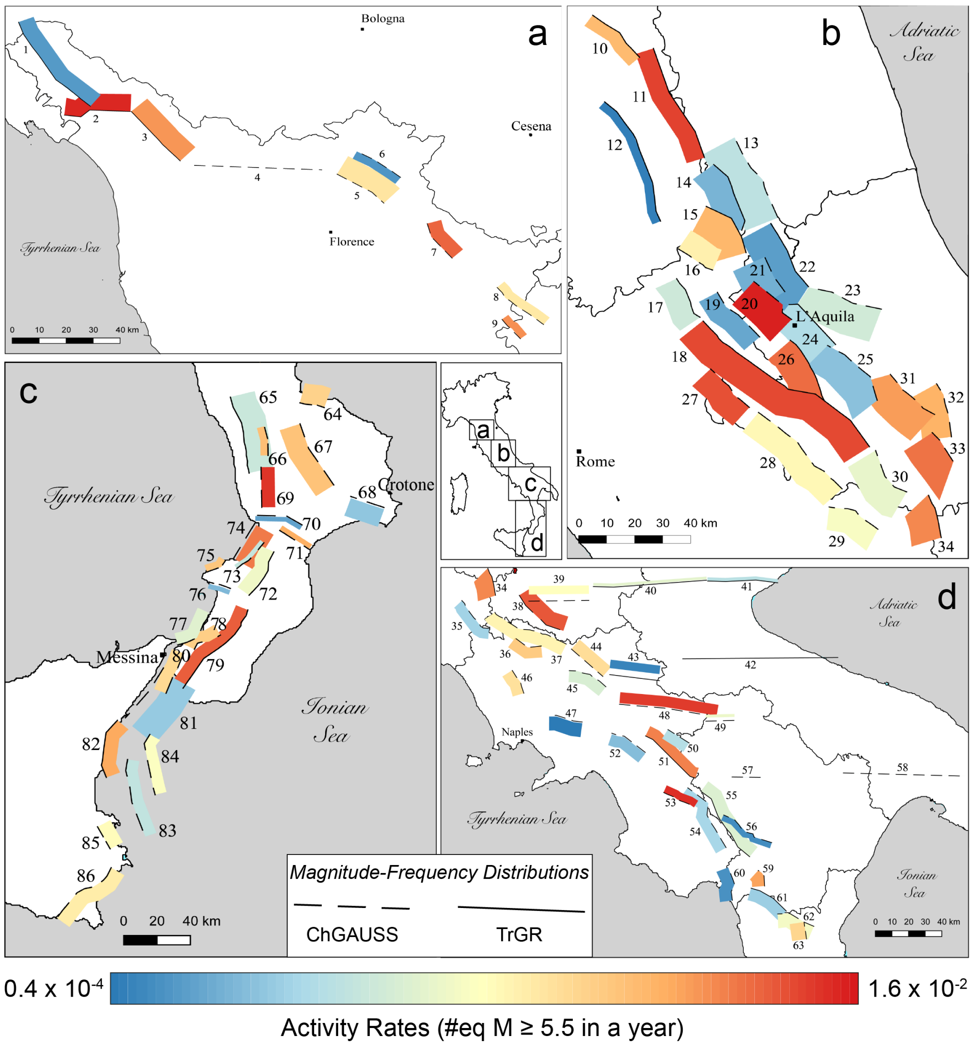

Fig. 3 Maps showing the fault source model as seismogenic boxes (see Fig. 2a). Colour scale indicates activity rate. Solid and dashed lines (in correspondence of the uppermost edge of the fault) are used to highlight our choice between the two end-members of magnitude-frequency distributions adopted here for the so-called *Mixed* model.

Nat. Hazards Earth Syst. Sci. Discuss., doi:10.5194/nhess-2017-41, 2017
Manuscript under review for journal Nat. Hazards Earth Syst. Sci.
Published: 6 February 2017

Natural Hazards and Earth System Sciences
Open Access
Discussions

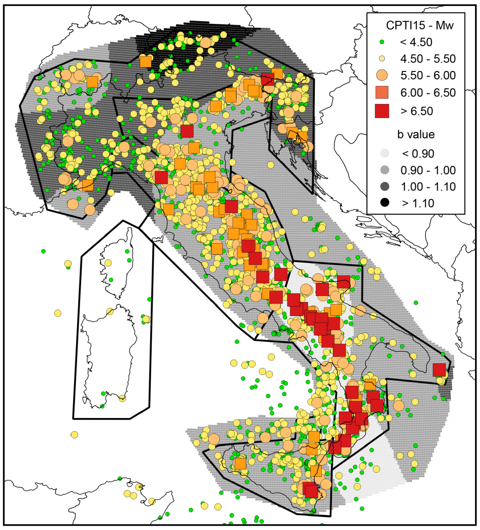

Fig. 4 Historical earthquakes from the most recent version of the historical parametric Italian catalogue (CPTI15, Rovida et al., 2016), the spatial variation in b-values and the polygons defining the five macroseismic areas used to assess magnitude completeness intervals.

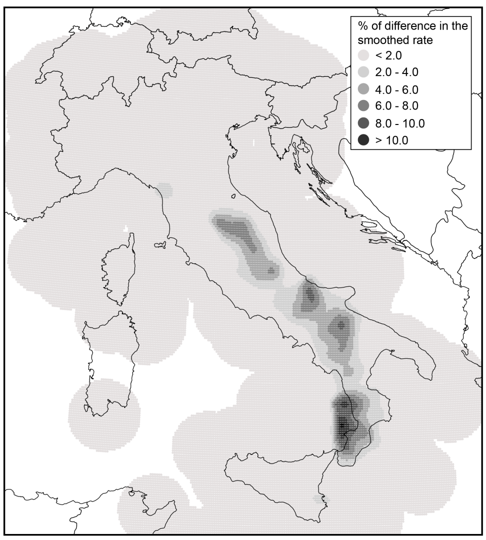

Fig. 5 Differences in percentages between the two smoothed rates produced by eq. (1) using the complete catalogue and the modified catalogue without events associated with known active faults (*TGR* model).

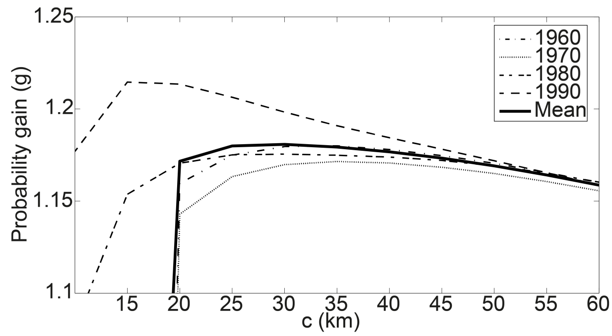

Fig. 6 Probability gain per earthquake (see eq. 2) versus c, showing the best radius for use in the smoothed seismicity approach (eq. 1).

Nat. Hazards Earth Syst. Sci. Discuss., doi:10.5194/nhess-2017-41, 2017
Manuscript under review for journal Nat. Hazards Earth Syst. Sci.
Published: 6 February 2017

Natural Hazards and Earth System Sciences
Open Access
Discussions

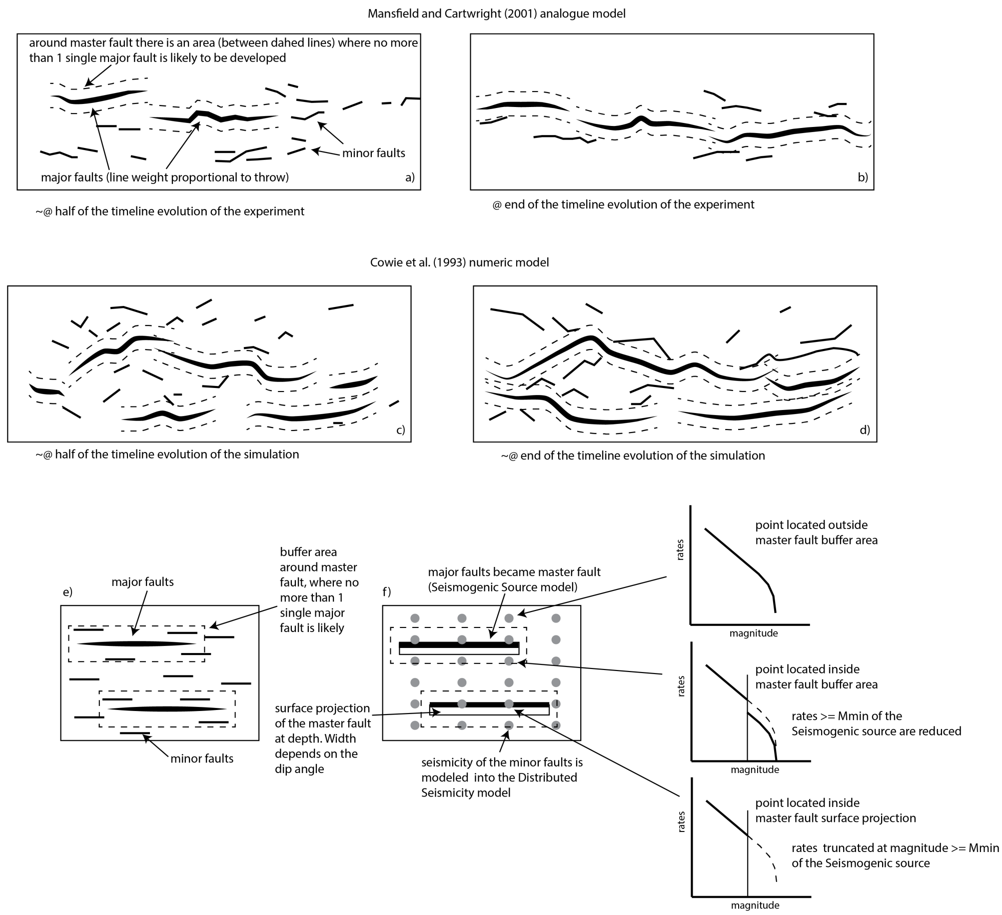

Fig. 7 Fault system evolution and implications in our model. a) and b) Sketches from the Mansfield and Cartwright (2001) analogue experiment at two different stages: approximately the midpoint of the sequence and the end of the sequence. Around master faults, there is an area where no more than a single major fault is likely to develop. c) and d) Sketches from numerical modelling conducted by Cowie et al. (1993) at two different stages. This experiment shows the similar evolutional features of major and minor faults. e) and f) Application of analogue and numerical modelling of fault system evolution to the fault source model proposed in this paper. A buffer area is drawn around each fault source, where it is unlikely for other major faults to develop, taking into account the length and slip rate of the fault source. This buffer area is useful for reducing or truncating the rates of expected seismicity of the distributed seismicity, depending on the position of a distributed seismicity point with respect to the buffer zone (see the text for details).

Nat. Hazards Earth Syst. Sci. Discuss., doi:10.5194/nhess-2017-41, 2017
Manuscript under review for journal Nat. Hazards Earth Syst. Sci.
Published: 6 February 2017

Natural Hazards and Earth System Sciences
Open Access
Discussions

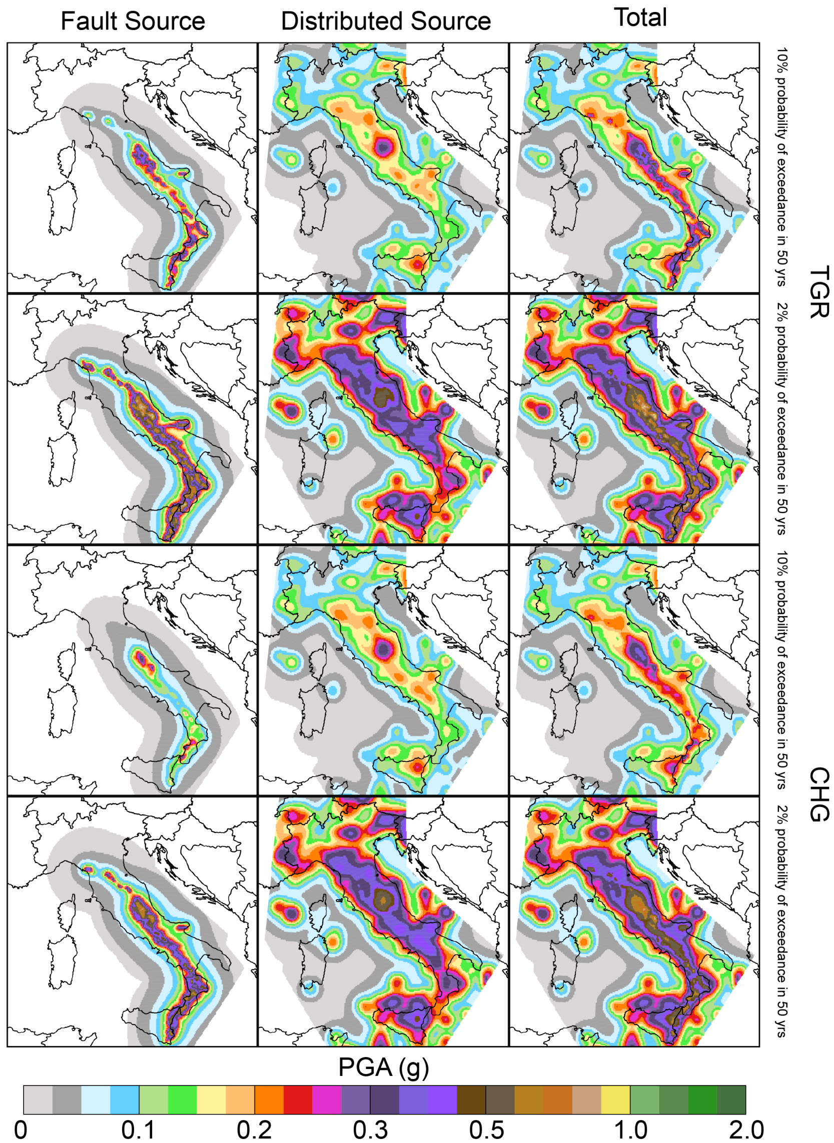

Fig. 8 Seismic hazard maps for the *TGR* and *CHG* models expressed in terms of peak ground acceleration (PGA) and computed for a latitude/longitude grid spacing of 0.05°. The first and second rows show the Fault Source, Distributed Source and Total maps for the *TGR* model, computed for 10% probability of exceedance in 50 years and for 2% probability of exceedance in 50 years, corresponding to return periods of 475 and 2475 years, respectively. The third and fourth rows show the same maps for the *CHG* model.

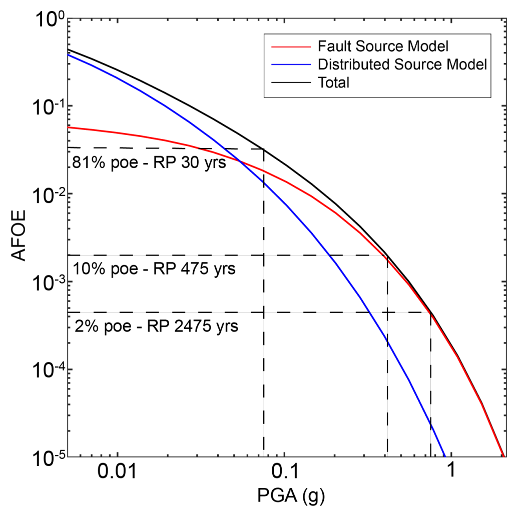

883

884 Fig. 9 An example of the contribution to the total seismic hazard (black line), in terms
885 of hazard curves, by the *fault* (red line) and *distributed* (blue line) source models for
886 one of the 45,602 grid points (L'Aquila, 42.400-13.400).
887
888

Nat. Hazards Earth Syst. Sci. Discuss., doi:10.5194/nhess-2017-41, 2017
Manuscript under review for journal Nat. Hazards Earth Syst. Sci.
Published: 6 February 2017

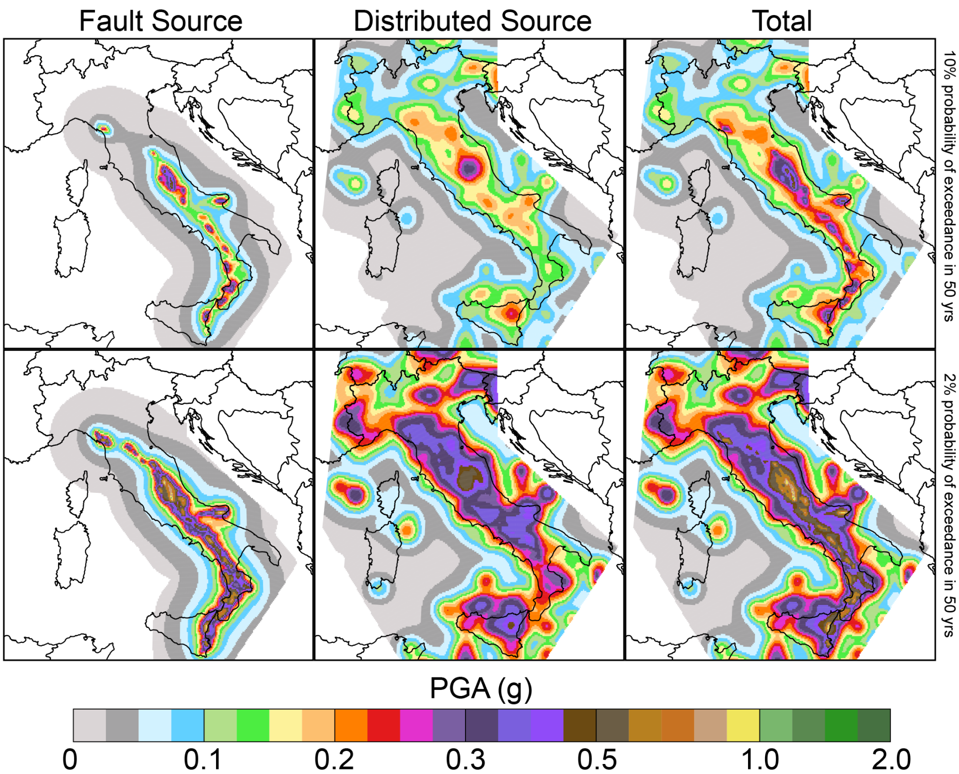

Fig. 10 Seismic hazard maps for the *Mixed* model. The first row shows the Fault Source, Distributed Source and Total maps computed for 10% probability of exceedance in 50 years, and the second row shows the same maps but computed for 2% probability of exceedance in 50 years, corresponding to return periods of 475 and 2475 years, respectively. The results are expressed in terms of peak ground acceleration (PGA).

Nat. Hazards Earth Syst. Sci. Discuss., doi:10.5194/nhess-2017-41, 2017
Manuscript under review for journal Nat. Hazards Earth Syst. Sci.
Published: 6 February 2017

Natural Hazards and Earth System Sciences
Discussions
Open Access

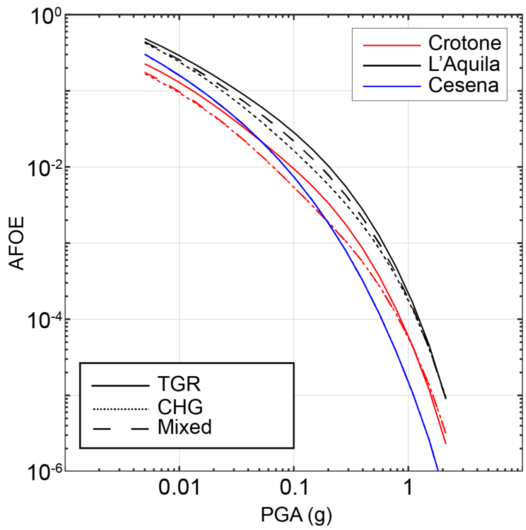

Fig. 11 *CHG* (dotted line), *TGR* (solid line) and *Mixed* model (dashed line) hazard curves for three sites: Cesena (red line), L'Aquila (black line) and Crotone (blue line).

Nat. Hazards Earth Syst. Sci. Discuss., doi:10.5194/nhess-2017-41, 2017
Manuscript under review for journal Nat. Hazards Earth Syst. Sci.
Published: 6 February 2017

Natural Hazards and Earth System Sciences
Open Access
Discussions

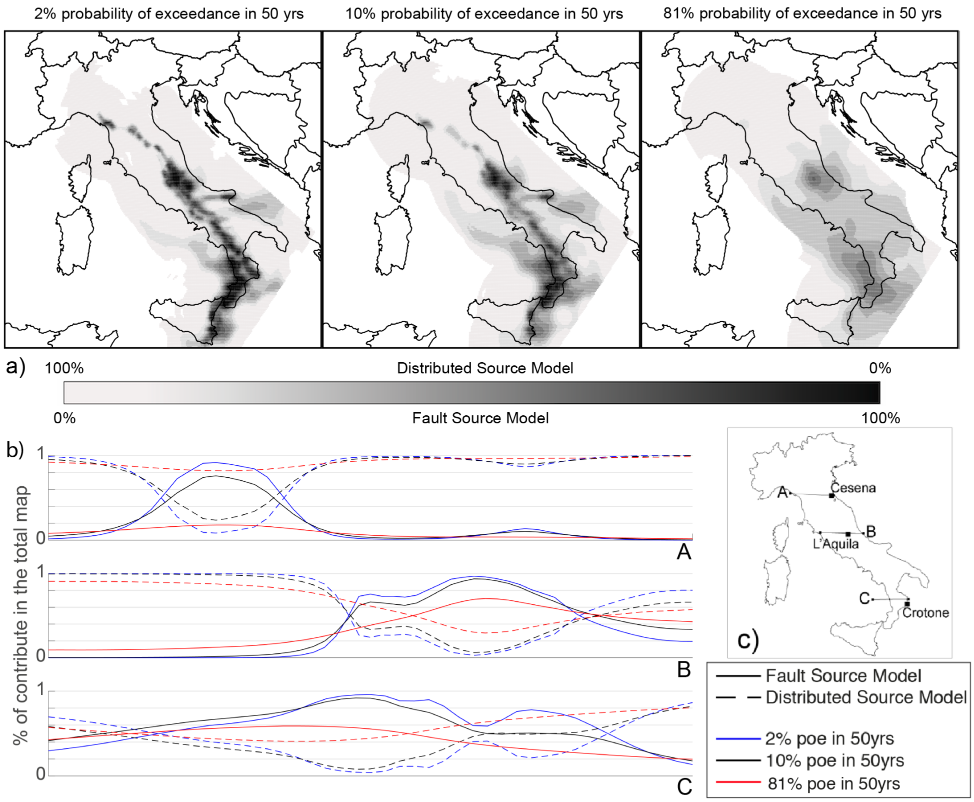

Fig. 12 a) Contribution maps of the Mixed *fault* source model and Mixed *distributed* source model to the total hazard for three probabilities of exceedance: 2%, 10% and 81%, corresponding to return periods of 2475, 475 and 30 years, respectively. b) Contributions of the Mixed *fault* (solid line) and Mixed *distributed* (dashed line) source models along three profiles (A, B and C in Fig. 12c) for three probabilities of exceedance: 2% (blue line), 10% (black line) and 81% (red line).

Nat. Hazards Earth Syst. Sci. Discuss., doi:10.5194/nhess-2017-41, 2017
Manuscript under review for journal Nat. Hazards Earth Syst. Sci.
Published: 6 February 2017

id	Fault Sources	L (km)	Dip (°)	Upper (km)	Lower (km)	SR_{min} (mm/yr)	SR_{max} (mm/yr)
1	Lunigiana	43.8	40	0	5	0.28	0.7
2	North Apuane Transfer	25.5	45	0	7	0.33	0.83
3	Garfagnana	26.9	30	0	4.5	0.35	0.57
4	Garfagnana Transfer	47.1	90	2	7	0.33	0.83
5	Mugello	21.0	40	0	7	0.33	0.83
6	Ronta	19.3	65	0	7	0.17	0.5
7	Poppi	17.1	40	0	4.5	0.33	0.83
8	Città di Castello	22.9	40	0	3	0.25	1.2
9	M.S.M. Tiberina	10.5	40	0	2.5	0.25	0.75
10	Gubbio	23.6	50	0	6	0.4	1.2
11	Colfiorito System	45.9	50	0	8	0.25	0.9
12	Umbra Valley	51.1	55	0	4.5	0.4	1.2
13	Vettore-Bove	35.4	50	0	15	0.2	1.05
14	Nottoria-Preci	29.0	50	0	12	0.2	1
15	Cascia-Cittareale	24.3	50	0	13.5	0.2	1
16	Leonessa	14.9	55	0	12	0.1	0.7
17	Rieti	17.6	50	0	10	0.25	0.6
18	Fucino	82.3	50	0	13	0.3	1.6
19	Sella di Corno	23.1	60	0	13	0.35	0.7
20	Pizzoli-Pettino	21.3	50	0	14	0.3	1
21	Montereale	15.1	50	0	14	0.25	0.9
22	Gorzano	28.1	50	0	15	0.2	1
23	Gran Sasso	28.4	50	0	15	0.35	1.2
24	Paganica	23.7	50	0	14	0.4	0.9
25	Middle Aternum Valley	29.1	50	0	14	0.15	0.45
26	Campo Felice-Ovindoli	26.2	50	0	13	0.2	1.6
27	Carsoli	20.5	50	0	11	0.35	0.6
28	Liri	42.5	50	0	11	0.3	1.26
29	Sora	20.4	50	0	11	0.15	0.45
30	Marsicano	20.0	50	0	13	0.25	1.2
31	Sulmona	22.6	50	0	15	0.6	1.35
32	Maiella	21.4	55	0	15	0.7	1.6
33	Aremogna C.Miglia	13.1	50	0	15	0.1	0.6
34	Barrea	17.1	55	0	13	0.2	1
35	Cassino	24.6	60	0	11	0.25	0.5
36	Ailano-Piedimonte	17.6	60	0	12	0.15	0.35
37	Matese	48.3	60	0	13	0.2	1.9
38	Bojano	35.5	55	0	13	0.2	0.9
39	Frosolone	36.1	70	11	25	0.35	0.93
40	Ripabottoni-San Severo	68.3	85	6	25	0.1	0.5
41	Mattinata	42.3	85	0	25	0.7	1
42	Castelluccio dei Sauri	93.2	90	11	22	0.1	0.5
43	Ariano Irpino	30.1	70	11	25	0.35	0.93
44	Tammaro	25.0	60	0	13	0.35	0.93
45	Benevento	25.0	55	0	10	0.35	0.93
46	Volturno	15.7	60	1	13	0.23	0.57
47	Avella	20.5	55	1	13	0.2	0.7
48	Ufita-Bisaccia	59.0	64	1.5	15	0.35	0.93
49	Melfi	17.2	80	12	22	0.1	0.5
50	Irpinia Antithetic	15.0	60	0	11	0.2	0.53

Nat. Hazards Earth Syst. Sci. Discuss., doi:10.5194/nhess-2017-41, 2017
Manuscript under review for journal Nat. Hazards Earth Syst. Sci.
Published: 6 February 2017

51	Irpinia	39.7	65	0	14	0.3	2.5
52	Volturara	23.7	60	1	13	0.2	0.35
53	Alburni	20.4	60	0	8	0.35	0.7
54	Caggiano-Diano Valley	46.0	60	0	12	0.35	1.15
55	Pergola-Maddalena	50.6	60	0	12	0.20	0.93
56	Agri	34.9	50	5	15	0.8	1.3
57	Potenza	17.8	90	15	21	0.1	0.5
58	Palagianello	73.3	90	13	22	0.1	0.5
59	Monte Alpi	10.9	60	0	13	0.35	0.9
60	Maratea	21.6	60	0	13	0.46	0.7
61	Mercure	25.8	60	0	13	0.2	0.6
62	Pollino	23.8	60	0	15	0.22	0.58
63	Castrovillari	10.3	60	0	15	0.2	1.15
64	Rossano	14.9	60	0	22	0.5	0.6
65	Crati West	49.7	45	0	15	0.84	1.4
66	Crati East	18.4	60	0	8	0.75	1.45
67	Lakes	43.6	60	0	22	0.75	1.45
68	Fuscalto	21.1	60	2	22	0.75	1.45
69	Piano Lago-Decollatura	25.0	60	1	15	0.23	0.57
70	Catanzaro North	29.5	80	3	20	0.75	1.45
71	Catanzaro South	21.3	80	3	20	0.75	1.45
72	Serre	31.6	60	0	15	0.7	1.15
73	Vibo	23.0	80	0	15	0.75	1.45
74	Sant'Eufemia Gulf	24.8	40	1	11	0.11	0.3
75	Capo Vaticano	13.7	60	0	8	0.75	1.45
76	Coccorino	13.3	70	3	11	0.75	1.45
77	Scilla	29.7	60	0	13	0.8	1.5
78	Sant'Eufemia	19.2	60	0	13	0.75	1.45
79	Cittanova-Armo	63.8	60	0	13	0.45	1.45
80	Reggio Calabria	27.2	60	0	13	0.7	2
81	Taormina	38.7	30	3	13	0.9	2.6
82	Acireale	39.4	60	0	15	1.15	2.3
83	Western Ionian	50.1	65	0	15	0.75	1.45
84	Eastern Ionian	39.3	65	0	15	0.75	1.45
85	Climiti	15.7	60	0	15	0.75	1.45
86	Avola	46.9	60	0	16	0.8	1.6

Table 1 Geometric Parameters of the Fault Sources. L, along-strike length; Dip, inclination angle of fault plane; Upper and Lower, representing the thickness of the local seismogenic layer; SRmin and SRmax are the slip rates assigned to the sources using the references available (see the supplements). *Id* is the identification of fault number.

Nat. Hazards Earth Syst. Sci. Discuss., doi:10.5194/nhess-2017-41, 2017
Manuscript under review for journal Nat. Hazards Earth Syst. Sci.
Published: 6 February 2017

Natural Hazards and Earth System Sciences
Open Access
Discussions

		Historical Earthquakes					Instrumental Earthquakes	
Id	Fault Sources	yyyy/mm/dd	I_{Max}	I_0	M_w	sD	yyyy/mm/dd	M_w
1	Lunigiana	1481/05/07	VIII	VIII	5.6	0.4		
		1834/02/14	IX	IX	6.0	0.1		
2	North Apuane Transfer	1837/04/11	X	IX	5.9	0.1		
3	Garfagnana	1740/03/06	VIII	VIII	5.6	0.2		
		1920/09/07	X	X	6.5	0.1		
4	Garfagnana Transfer							
5	Mugello	1542/06/13	IX	IX	6.0	0.2		
		1919/06/29	X	X	6.4	0.1		
6	Ronta							
7	Poppi							
8	Città di Castello	1269			5.7			
		1389/10/18	IX	IX	6	0.5		
		1458/04/26	VIII-IX	VIII-IX	5.8	0.5		
		1789/09/30	IX	IX	5.9	0.1		
9	M.S.M. Tiberina	1352/12/15	IX	IX	6.3	0.2		
		1917/04/26	IX-X	IX-X	6.0	0.1		
10	Gubbio						1984/04/29	5.6
11	Colfiorito System	1279/04/30	X	IX	6.2	0.2	1997/09/26	5.7
		1747/04/17	IX	IX	6.1	0.1	1997/09/26	6
		1751/07/27	X	X	6.4	0.1		
12	Umbra Valley	1277		VIII	5.6	0.5		
		1832/01/13	X	X	6.4	0.1		
		1854/02/12	VIII	VIII	5.6	0.3		
13	Vettore-Bove							
14	Nottoria-Preci	1328/12/01	X	X	6.5	0.3	1979/09/19	5.8
		1703/01/14	XI	XI	6.9	0.1		
		1719/06/27	VIII	VIII	5.6	0.3		
		1730/05/12	IX	IX	6.0	0.1		
		1859/08/22	VIII-IX	VIII-IX	5.7	0.3		
		1879/02/23	VIII	VIII	5.6	0.3		
15	Cascia-Cittareale	1599/11/06	IX	IX	6.1	0.2		
		1916/11/16	VIII	VIII	5.5	0.1		
16	Leonessa							
17	Rieti	1298/12/01	X	IX-X	6.3	0.5		
		1785/10/09	VIII-IX	VIII-IX	5.8	0.2		
18	Fucino	1349/09/09	IX	IX	6.3	0.1		
		1904/02/24	IX	VIII-IX	5.7	0.1		
		1915/01/13	XI	XI	7	0.1		
19	Sella di Corno							
20	Pizzoli-Pettino	1703/02/02	X	X	6.7	0.1		
21	Montereale							
22	Gorzano	1639/10/07	X	IX-X	6.2	0.2		
		1646/04/28	IX	IX	5.9	0.4		
23	Gran Sasso							
24	Paganica	1315/12/03	VIII	VIII	5.6	0.5	2009/06/04	6.3
		1461/11/27	X	X	6.5	0.5		
25	Middle Aternum Valley							
26	Campo Felice-Ovindoli							
27	Carsoli							
28	Liri							
29	Sora	1654	X	IX-X	6.3	0.2		
30	Marsicano							
31	Sulmona							
32	Maiella							
33	Aremogna C.Miglia							
34	Barrea						1984/05/07	5.9
35	Cassino							
36	Ailano-Piedimonte							
37	Matese	1349/09/09	X-XI	X	6.8	0.2		

Nat. Hazards Earth Syst. Sci. Discuss., doi:10.5194/nhess-2017-41, 2017
Manuscript under review for journal Nat. Hazards Earth Syst. Sci.
Published: 6 February 2017

Natural Hazards and Earth System Sciences
Open Access
Discussions

38	Bojano	1805/07/26	X	X	6.7	0.1		
39	Frosolone	1456/12/05	XI	XI	7	0.1		
40	Ripabottoni-San Severo	1627/07/30	X	X	6.7	0.1	2002/10/31	5.7
		1647/05/05	VII-VIII	VII-VIII	5.7	0.4		
		1657/01/29	IX-X	VIII-IX	6.0	0.2		
41	Mattinata	1875/12/06	VIII	VIII	5.9	0.1		
		1889/12/08	VII	VII	5.5	0.1		
		1948/08/18	VII-VIII	VII-VIII	5.6	0.1		
42	Castelluccio dei Sauri	1361/07/17	X	IX	6	0.5		
		1560/05/11	VIII	VIII	5.7	0.5		
		1731/03/20	IX	IX	6.3	0.1		
43	Ariano Irpino	1456/12/05			6.9	0.1		
		1962/08/21	IX	IX	6.2	0.1		
44	Tammaro	1688/06/05	XI	XI	7	0.1		
45	Benevento							
46	Volturno							
47	Avella	1499/12/05	VIII	VIII	5.6	0.5		
48	Ufita-Bisaccia	1732/11/29	X-XI	X-XI	6.8	0.1		
		1930/07/23	X	X	6.7	0.1		
49	Melfi	1851/08/14	X	X	6.5	0.1		
50	Irpinia Antithetic							
51	Irpinia	1466/01/15	VIII-IX	VIII-IX	6.0	0.2	1980/11/23	6.8
		1692/03/04	VIII	VIII	5.9	0.4		
		1694/09/08	X	X	6.7	0.1		
		1853/04/09	IX	VIII	5.6	0.2		
52	Volturara							
53	Alburni							
54	Caggiano-Diano Valley	1561/07/31	IX-X	X	6.3	0.1		
55	Pergola-Maddalena	1857/12/16			6.5			
		1857/12/16			6.3			
56	Agri							
57	Potenza	1273/12/18	VIII-IX	VIII-IX	5.8	0.5	1990/05/05	5.8
58	Palagianello							
59	Monte Alpi							
60	Maratea							
61	Mercure	1708/01/26	VIII-IX	VIII	5.6	0.6	1998/09/09	5.5
62	Pollino							
63	Castrovillari							
64	Rossano	1836/04/25	X	IX	6.2	0.2		

Nat. Hazards Earth Syst. Sci. Discuss., doi:10.5194/nhess-2017-41, 2017
Manuscript under review for journal Nat. Hazards Earth Syst. Sci.
Published: 6 February 2017

Natural Hazards and Earth System Sciences
Open Access
EGU
Discussions

65	Crati West	1184/05/24	IX	IX	6.8	0.3
		1870/10/04	X	IX-X	6.2	0.1
		1886/03/06	VII-VIII	VII-VIII	5.6	0.3
66	Crati East	1767/07/14	VIII-IX	VIII-IX	5.9	0.2
		1835/10/12	X	IX	5.9	0.3
67	Lakes	1638/06/08	X	X	6.8	0.1
68	Fuscalto	1832/03/08	X	X	6.6	0.1
69	Piano Lago-Decollatura					
70	Catanzaro North	1638/03/27			6.6	
71	Catanzaro South	1626/04/04	X	IX	6.1	0.4
72	Serre	1659/11/05	X	X	6.6	0.1
		1743/12/07	IX-X	VIII-IX	5.9	0.2
		1783/02/07	X-XI	X-XI	6.7	0.1
		1791/10/13	IX	IX	6.1	0.1
73	Vibo					
74	Sant'Eufemia Gulf	1905/09/08	X-XI	X-XI	7	0.1
75	Capo Vaticano					
76	Coccorino	1928/03/07	VIII	VII-VIII	5.9	0.1
77	Scilla					
78	Sant'Eufemia	1894/11/16	IX	IX	6.1	0.1
79	Cittanova-Armo	1509/02/25	IX	VIII	5.6	0.4
		1783/02/05	XI	XI	7.1	0.1
80	Reggio Calabria					
81	Taormina	1908/12/28	XI	XI	7.1	0.2
82	Acireale	1818/02/20	IX-X	IX-X	6.3	0.1
83	Western Ionian	1693/01/11	XI	XI	7.3	0.1
84	Eastern Ionian					
85	Climiti					
86	Avola					

Table 2 Earthquake-Source Association Adopted for Fault Sources. $I_{Max,}$ maximum intensity; I_0, epicentral intensity; M_w, moment magnitude; sD, standard deviation of the moment magnitude. For the references see the supplement file.